Technical Report ARWEC-TR-01005

AN EXPLOSIVE CHARGE WITH COMPLEX LINER PROFILE

Vladimir M. Gold

August 2001

US ARMY
TANK AUTOMOTIVE AND
ARMAMENTS COMMAND
ARMAMENT RDE CENTER

U.S. ARMY ARMAMENT RESEARCH, DEVELOPMENT AND ENGINEERING CENTER

Warheads, Energetics & Combat-support Armament Center

Picatinny Arsenal, New Jersey

The views, opinions, and/or findings contained in this report are those of the author(s) and should not be construed as an official Department of the Army position, policy, or decision, unless so designated by other documentation.

The citation in this report of the names of commercial firms or commercially available products or services does not constitute official endorsement by or approval of the U.S. Government.

Destroy this report when no longer needed by any method that will prevent disclosure of its contents or reconstruction of the document. Do not return to the originator.

REPORT DOCUMENTATION PAGE

Form Approved
OMB No. 0704-01-0188

PLEASE DO NOT RETURN YOUR FORM TO THE ABOVE ADDRESS.

1. REPORT DATE *(DD-MM-YYYY)*	2. REPORT TYPE	3. DATES COVERED *(From - To)*
August 2001	Final	20 October 1998

4. TITLE AND SUBTITLE

AN EXPLOSIVE CHARGE WITH COMPLEX LINER PROFILE

5a. CONTRACT NUMBER

5b. GRANT NUMBER

5c. PROGRAM ELEMENT NUMBER

6. AUTHORS

Vladimir M. Gold

5d. PROJECT NUMBER

5e. TASK NUMBER

5f. WORK UNIT NUMBER

7. PERFORMING ORGANIZATION NAME(S) AND ADDRESS(ES)

ARDEC, WECAC
Energetics & Warheads Division (AMSTA-AR-WEE-C)
Picatinny Arsenal, NJ 07806-5000

8. PERFORMING ORGANIZATION REPORT NUMBER

9. SPONSORING/MONITORING AGENCY NAME(S) AND ADDRESS(ES)

ARDEC, WECAC
Information Research Center (AMSTA-AR-WEL-T)
Picatinny Arsenal, NJ 07806-5000

10. SPONSOR/MONITOR'S ACRONYM(S)

11. SPONSOR/MONITOR'S REPORT NUMBER(S)

Technical Report ARWEC-TR-01005

12. DISTRIBUTION/AVAILABILITY STATEMENT

Approved for public release; distribution is unlimited.

13. SUPPLEMENTARY NOTES

14. ABSTRACT

A considerable amount of the energy released from the detonation of an explosive charge can be captured using a metal liner, which then can be focused to form a projectile for boring a hole in a target. Such a hole drilling explosive charge is frequently used in demolition operations for rapid boring of holes, which have to permit insertion or passage of fixed diameter main demolition charges. Because of the stringent hole requirements, the penetrator that is ideally suited for these applications has to consist of two separate penetrators: a hole driller and a hole cleaner. The shape and the parameters of this complex penetrator are crucial for the charge effectiveness. This work offers a detailed discussion on a number of basic issues involved in designing a liner profile that is capable of producing such a penetrator. Based on results of numerical experimentation, the validity of a design rationale that formation of the hole driller and hole cleaner are mutually independent was established and proven experimentally. Numerical (cont'd)

15. SUBJECT TERMS

Explosive charge, Liner, Explosively formed penetrator, Shaped charge, Demolition

16. SECURITY CLASSIFICATION OF:			17. LIMITATION OF ABSTRACT	18. NUMBER OF PAGES	19a. NAME OF RESPONSIBLE PERSON
a. REPORT	b. ABSTRACT	c. THIS PAGE			19B. TELEPHONE NUMBER *(Include area code)*
UNCLASSIFIED	UNCLASSIFIED	UNCLASSIFIED	UNCLASSIFIED	32	

13. **ABSTRACT** (cont'd)

simulations confirmed the validity of the accepted design rationale; experiments indicated good agreement with the simulations and proved the feasibility of producing a robust penetrator of this complex shape.

ACKNOWLEDGMENTS

We acknowledge Mr. Joseph . Turci of the U.S. Army Armaments Research, Development and Engineering Center, Picatinny Arsenal, NJ and Mr. Russel L. Amdor of Battelle for directing and conducting the experiments.

CONTENTS

FIGURES

NOMENCLATURE

e_l	Directional unit vector of a straight line connecting point masses m_1 and m_2
$e_r, e_q,$ and e_z	A triad of mutually orthogonal unit vector. Radial, out of plane, and axial unit vectors.
E	Energy
F' and F''	Forces at liner curvature discontinuity
F_1 and F_2	Initial forces applied to masses m_1 and m_2
G, G_0	Torque, initial torque
H	Angular momentum
m_1 and m_2	Point masses of an idealized two mass system
M' and M''	Momenta at liner curvature of discontinuity
M_1 and M_2	Initial momenta applied to point masses m_1 and m_2
$M_0, M_{0r},$ and M_{0z}	Magnitude of the total initial liner momentum and its radial and axial components
n	Unit vector normal to liner rear surface
p	Pressure
$p = p(\xi, t)$	Pressure at liner rear surface
r	Radial coordinate
$R(\xi)$	Profile of liner rear surface
R_{cm}	Position of center of mass of liner profile
s_{ij}	Stress deviator
t	Time
υ_r and υ_z	Radial and axial velocity components
z	Axial coordinate

$\alpha = \alpha(\xi)$	Liner angle
α_1 and α_2	Liner angle at points 1 (inner edge) and 2 (outer edge)
δ	Variation
$\delta\alpha_1$	Variation of liner angle α_1
δR	Liner profile variation
δz_1 and δz_2	Variation of axial coordinates of liner edge 1 and 2, respectively
$\dot{\varepsilon}$	Stretching rate
ρ	Density
$\sigma_{ij}, \sigma_{rr}, \sigma_{rz}, \sigma_{zz}$	Stress tensor; stress tensor components
τ	Relaxation time
ξ	Dimensionless coordinate along liner profile, $0 \le \xi \le 1$
$\varphi(\xi), \psi(\xi)$	Blending functions

INTRODUCTION

A considerable amount of the energy released from the detonation of an explosive charge can be captured using a metal liner, which then can be focused to form a projectile for boring a hole in a target. A typical device, referred to as a shaped charge (SC), consists of an explosive charge formed with a cavity, which is lined with a thin layer of metal. When the charge is detonated, the resulting pressure collapses the metal liner and forms it into a high-speed projectile. Depending on the explosive and the mass and geometry of the liner, projectiles can attain velocities varying between 1.5 and 12 km/s. When such a high-speed projectile interacts with a solid, it is capable of penetrating it, and this effect is employed in a number of military and industrial applications.

Typically, SCs are employed either (1) at short (a few charge diameters) or (2) at long distances (tens or hundreds of charge diameters) from the target, in which case they are often referred to at explosively formed penetrators (EFPs). Although the term "explosively formed penetrators" implies a reference to a projectile (employed as a penetrator) produced from an explosive charge (i.e., shaped charge), an accepted usage of this term applies to a charge with a smooth shallow liner profile. The terminology used in this paper will follow this practice.

Because of the different standoffs for different applications, times available for the projectile formation can be markedly different. However, in order to maximize target penetration, penetrator length has to be maximized. Thus for most applications, the given standoff (or time) to form a penetrator before striking the target is the most important constraint for maximizing projectile length. These considerations determine SC (or EFP) effectiveness, and therefore, play a crucial role in choosing an appropriate liner design rationale.

In principle, independent of the liner shape, liner acceleration is carried out very rapidly compared with the time allowed for projectile formation; therefore, the effectiveness of the energy transfer from the explosive to liner (or resulting projectile) is virtually independent of the target standoff. Another fact that is important in liner design is that the momentum transferred to a liner is a fixed function of the explosive type, liner thickness (mass), and the charge boundary conditions, and the magnitude of the momentum is not significantly affected by small variations in liner shape. Nevertheless, the dynamics of liner collapse and projectile formation is very sensitive to the liner shape and thickness. Therefore, the adjustment of liner shape is a common design technique for the control of projectile formation time.

For example, in short-range SC applications, where the time for the formation of a long projectile is limited, the liner is designed in a way that the tip of the resulting projectile (often called a jet) moves much faster than the tail. This results in a stretching projectile, which continues to gain length even as its tip penetrates the target. If the stretching continues, as it would in long standoff applications, the projectile would ultimately fracture. This can significantly degrade target penetration. Therefore, for long-range (EFP) applications, the design criterion is to achieve long and stable (non-stretching) projectile.

The employment of various SC designs depends on specific applications, and the examples of these applications are numerous. During the Second World War, a number of antitank weapons (e.g., the rocket-propelled Bazooka) were developed which made use of short-range SCs to perforate thick metal plates (ref. 1). A historical outline of the developments in shaped charge technology

is given by Kennedy (ref. 2). Recent long-range EFP developments for antitank weapons are reviewed by Hornemann et al. (ref. 3) and Weimann (ref. 4). Charges lined with linear wedges (linear SC) have been used for cutting cables and bridge beams and in salvage work on sunken ships.

Various explosive charges are commonly used in mining operations to break large rocks. Short range SCs have frequently been used for the rapid boring of holes for demolition work. After a hole has been produced with a SC, the cavity can be filled with explosive for further blasting. Some of these applications (ref. 5) have stringent requirements for the bored holes, which have to permit insertion or passage of a fixed diameter main demolition charge. This paper discusses a number of the issues involved in the development of a special single SC, which produces a complex penetrator that should be ideally suited for these applications. The proposed complex penetrator introduced in this work has two separate parts:

- A stretching central solid rod penetrator (referred to in this work as a hole "driller")
- A concentrate, radially stable and non-stretching hollow cylindrical penetrator (referred to in this work as a hole "cleaner")

Our experiments confirmed that it is possible to produce a robust penetrator of this complex shape. The following is a detailed discussion of a number of issues involved in designing this SC.

PENETRATOR'S SHAPE

Structures that are encountered in demolition operations are made from a variety of geologic and man-made materials and are usually reinforced with steel. When a simple rod penetrates such a target, the resulting hole diameters vary as the penetrator penetrates different materials. Ductile metals are ideally suited for witnessing this effect. Birkhoff et al. (ref. 1), using a stack of alternating steel and lead plates, demonstrated a striking difference in hole diameters of adjacent plates: hole diameters in the lead, which is extremely weak, were four to five time larger than the much stronger steel. Similarly, when the target material is inhomogeneous and consists of a matrix of weak brittle materials containing metal inclusions, these effects are also significant. Appreciable differences in hole diameters between the embedded steel plates and the concrete were reported from penetration experiments with gun launched penetrators against simulated reinforced concrete targets (ref. 6).

In this type of target, reinforcing steel occupies only a small fraction of the total hole volume, but nevertheless controls the passage of the demolition charge. This requires special penetrator solutions to achieve satisfactory bore holes. When a hole is created with a simple rod penetrator in order to permit passage of a fixed diameter demolition charge, the penetrator's diameter has to be increased. This severely enlarges the hole in the weaker portions of the target. Such holes not only witness the poor efficiency of the penetrator, but, most importantly, degrade the effectiveness of the demolition charge by causing excessive venting of explosion products. Therefore, to ensure proper performance of the demolition charge, the hole has to be created with two penetrators: (1) a hole driller, which creates a nominal hole in the weaker material and (2) a hole cleaner, which cuts out remnants from the harder inclusions (steel, etc.). A variety of practical approaches are possible, and one of the solutions is to generate these penetrators using a single charge.

The objective here was to investigate a single charge that generates two penetrators: a central solid rod driller and a concentric hollow cylinder cleaner. The function of the hole driller is to create a nominal diameter hole. The deeper the burial of the demolition charge, the higher is the degree of the confinement of the explosive and the resulting transfer of the momentum to the target, which ultimately causes it failure. Therefore, increasing hole depth increases the effectiveness of the demolition charge. Because of practical considerations, the charge standoff is limited to a few charge diameters. Thus, in order to create a deep hole, the hole driller has to stretch as it penetrates the target. The second part of the penetrator, the concentric hollow cylinder acts as a hole cleaner. It should not attempt to cut through the main target material, but instead should follow the hole driller. Therefore, the hole cleaner has to have a slower velocity than the hole driller. Since a fixed diameter hole is required, the hole cleaner has to be radially stable; i.e., it should not continue to collapse or expand (radially) as it moves in the target.

To obtain these two radically different penetrators from a single charge is not a simple task. What is the liner shape that has to be used to obtain such a complex projectile? Figure 1 shows results of the numerical simulations of an initially attempted design. Both parts of the penetrator are unsatisfactory. In fact, the simulations suggest that the peripheral portion not only fails to form a robust penetrator, it does not even indicate a tendency to separate from the central part.

NUMERICAL SIMULATIONS

To produce this complex penetrator, the principle design rationale is to divide a liner into distinct central and peripheral portions that are to generate two separate penetrators; hole driller and hole cleaner, respectively. Typical SC and EFP liners produce penetrators that are somewhat similar to the two required; thus, the liner profile can be a blend of SC and EFP designs. To avoid costly experimentation with different liner profiles, numerical simulations are instrumental for examination of the correlation between the liner shape and the resulting penetrator. The principle step in this development process is to identify basic liner parameters, which control the shape and robustness of the desired penetrator. Then, based on observations learned from the simulations, an experimental charge is to be fabricated and tested, and the experimental data are to be compared with (and, hopefully, prove) the tendencies observed in the analysis. The specific objectives of numerical simulations conducted in this work were as follows:

- To obtain the desired hole driller with the required penetration parameter such as tip velocity, length, stretching rate, diameter, etc.
- To achieve liner separation into two robust parts with the minimum fragmentation losses
- To examine liner parameters that affect formation and stability of the desired hole cleaner

Numerical Model

The dynamics of a stretching SC liner collapse is radically different from a stable EFP formation. The projectile formation of a stable EFP is accomplished through a relatively moderate plastic deformation of the liner, similar to these experienced in metal forging. Modeling of these EFPs is usually carried out in a Lagrangian reference frame. For stretching SCs, the plastic deformation of

the liner is extremely severe. When a Lagrangian reference frame is employed in modeling stretching SCs, the computational mesh is severely distorted. This has an adverse effect on the integration time step on accuracy, which is directly related to the grid size through the Courant stability condition. Therefore, commonly, SC modeling is carried out using Eulerian computational mesh, which is fixed in space and is not subject to the Lagrangian mesh distortion problems.

In our problem, the penetrator consists of both a stable and a stretching part. Because of the mesh distortion of the stretching portion, purely Lagrangian modeling would not be acceptable. Although using a Eulerian reference frame would solve the mesh problems, the calculation of the lengthy formation of the stable part would require significant computational resources. The numerical simulations presented in this work were performed using the CALE (ref. 7) computer program.

CALE is a plane two-dimensional and three-dimensional axisymmetric hydrodynamics code basd on an Arbitrary Lagrangian Eulerian Formulation of the governing equations. It can run in a pure Lagrangian mode, a pure Eulerian mode, or in arbitrary hybrid mode. CALE is capable of modeling multi-material flows and allows for discontinuous velocities at material interfaces. In the Eulerian reference frame, the description of the axisymmetric kinematic deformation of the continuum is given by the following conservation laws:

Conservation of mass

$$\frac{\partial \rho}{\partial t}+\upsilon_r\frac{\partial \rho}{\partial r}+\upsilon_z\frac{\partial \rho}{\partial z}+\rho\left(\frac{1}{r}\frac{\partial}{\partial r}(r\upsilon_r)+\frac{\partial \upsilon_z}{\partial_z}\right)=0$$

Conservation of linear momentum

$$\frac{\partial \upsilon_r}{\partial t}+\upsilon_r\frac{\partial \upsilon_r}{\partial r}+\upsilon_z\frac{\partial \upsilon_r}{\partial z}=\frac{1}{\rho}\left(\frac{\partial \sigma_{rr}}{\partial r}+\frac{\partial}{\partial z}(\sigma_{rz}+p)+\frac{\sigma_{rr}+\sigma_{zz}+2p}{r}\right)$$

$$\frac{\partial \upsilon_r}{\partial t}+\upsilon_r\frac{\partial \upsilon_z}{\partial r}+\upsilon_z\frac{\partial \upsilon_z}{\partial z}=\frac{1}{\rho}\left(\frac{\partial \sigma_{zz}}{\partial z}+\frac{\partial}{\partial r}(\sigma_{rz}+p)+\frac{\sigma_{rz}+p}{r}\right)$$

Conservation of energy

$$\frac{\partial E}{\partial t}+v_r\frac{\partial E}{\partial r}+v_z\frac{\partial E}{\partial z}=\frac{1}{\rho}\left(-p\left(\frac{1}{r}\frac{\partial}{\partial r}(r\upsilon_r)+\frac{\partial \upsilon_z}{\partial z}\right)+r\frac{\partial}{\partial r}\left(\frac{\upsilon_r}{r}\right)(\sigma_{rr}+p)\right.$$

$$\left.+(\sigma_{zz}+p)\left(\frac{\partial \upsilon_z}{\partial z}-\frac{\upsilon_r}{r}\right)+(\sigma_{rz}+p)\left(\frac{\partial \upsilon_r}{\partial z}-\frac{\partial \upsilon_z}{\partial r}\right)\right)$$

Body forces (such as gravity), thermal energy sources, and heat conduction are ignored.

CALE's procedure for calculating elastic-plastic flow is based on the methodology developed by Wilkins (refs. 8 and 9). The stress behavior of a material can be thought of being composed of a stress associated with uniform hydrostatic pressure p, referred to as the spherical part of a stress

tensor, plus the stress associated with the resistance of the material to shear distortion, referred to as a deviator s_{ij}. In describing yielding and plastic flow, the stress contributions that are due to shear distortion are limited by the constitutive equation for the material. The stress tensor is given then by

$$\sigma_{ij} = -p + s_{ij}$$

The constitutive equation for the liner material adopted here is that of Steinberg-Guinan (ref. 10), which specifies the shear modulus and the yield strength as a function of pressure, temperature, and equivalent plastic strain. The hydrodynamic response of liner material was modeled with the standard linear polynomial approximation, usually employed for metals. The liner was modeled with a standard set of parameters for oxygen-free high conductivity (OFHC) copper, which were taken from Tipton (ref. 9). Details for these models and their implementation can be found in Tipton (ref. 8).

The explosive was modeled as an ideal hydrodynamic material ($s_{ij} = 0$), serving as an energy source. The procedure for modeling the explosive's energy release rate used the Jones-Wilkins-Lee (JWL) equation of state and a burn fraction algorithm based on a constant detonation velocity D_0 and a uniform chemical energy density e_0. Parameter values for LX-14 from Tipton (ref. 9) were used to model the explosive.

In addition to the specification of the material models, problem geometry and initial and boundary conditions have to be specified before the solution procedure can be initiated. The configuration of an axially symmetrical geometric domain in $r-z$ space is shown in figure 2. Domain $A_1E_1E_3E_2$ represents the explosive booster pellet, $E_2E_4E_5E_6E_7E_8$, is the main explosive, $E_8E_7E_6L_1L_2L_3$ is the copper liner, $R_1R_2R_3R_4$ is the steel confinement ring, and the rest of the domain $A_1A_2A_3A_4$ is filled with air.

The following boundary conditions were applied along the boundary of domain $A_1A_2A_3A_4$

υ_z = 0	along A_3A_4
σ_n = 0	along A_1A_2 and A_2A_3
υ_r = 0	along A_1A_4 (line of axial symmetry)

CALE is capable of modeling discontinuities in the tangential component of the velocity across material interfaces, and a so-called "slide line $E_6E_7E_8$ between the explosive and the liner was included in the model.

The explosive was detonated at the point A_1. The initial size of the computational domain was 95 zones in the z direction and 84 zones in the r direction. With the explosion, the boundary of the spatial domain expands. If the size of the computational domain (i.e., number of zones) was to be left unchanged with time, the motion of the stretching projectile that reached the boundary would have to be resolved on a limited region of the mesh. This would introduce great inaccuracies in the calculations. The axial component of the velocity at the boundary A_3A_4 (the air) was set to zero,

$v_z = 0$, until the projectile approached it at a distance of approximately 3 cm. At that time, 3 cm of new mesh containing 10 zones (in the z direction) were added to that boundary. Then, as the projectile moved onto the newly formed mesh approaching the new boundary, the procedure was repeated. The periodic addition of computational mesh was performed during the entire course of calculations.

Hole Driller

When the explosive detonates, it undergoes vigorous chemical decomposition that generates pressures in the order of two to four hundreds of Kbars. Since the ability of the detonation products to transmit shear is very small, the liner can be thought to be accelerated only under action of forces normal to its surface. By changing the orientation of the liner surface adjacent to the explosive, one can change the relative amounts of axial and radial components of the momentum imparted to the liner. Since the ensuing motion of the liner's material depends on the initial amounts of axial and radial momenta, the adjustment of liner angle α (fig. 3a) is a common technique for control of liner collapse and projectile formation.

Numerical simulations of liner collapse for different liner geometries are shown in figure 4. In order to produce the required stretching hole driller, we decreased (as compared to a liner shown in fig. 1) the liner angle α. Decreases in α increase the radial component of the momentum transferred to the liner. This causes the liner to undergo more intense radial deformation (fig. 4). Shaped charges shown in figure 4 have elliptic liner profiles, and their liner collapse mechanisms are very similar to the conical SCs (ref. 1). In order to illustrate the process of this type of projectile formation, one can apply a conservation of mass principle to the control volume occupied by the liner. Liner radial contraction generates an intense flow (or jet) in the axial direction. With respect to the center of mass, the axial flow is in two opposing directions and the difference in velocities is large. This is why this type of liner collapse mechanism produces a stretching solid rod-like projectile, and when the projectile (or jet) is viewed from a conventional stationary reference frame, axial velocity of the tip is much higher than of the tail.

Liner Separation into Two Robust Parts

The liner angle α can also be used to guide the direction of liner collapse in such a way that the liner would separate into two parts, central and peripheral (figs. 1 and 4). This is accomplished with the following technique. Along the line where the liner is to break, an edge is formed. At the edge, the two surfaces are given significantly different collapse angles (if the center has to stretch, $\alpha' < \alpha''$). The magnitudes of the momenta M' and M'' imparted to the two parts are the same, but their directions are different (fig. 3b and c). In the vicinity of the edge, when the two momenta are in opposing direction, the intense plastic flow leads to "necking." This ultimately causes the liner to separate into two parts.

What liner parameters can be adjusted to control the separation process? Suppose the liner would break along an idealized necking plane given by an angle β. The necking is driven by two forces $F' = \partial M' / \partial t$ and $F'' = \partial M'' / \partial t$, and the separation occurs only when the forces pull the two parts in opposing directions. Therefore, the necessary condition for the separation is the $(F' \cdot n)(F'' \cdot n) < 0$, which requires $\alpha' < \beta < \alpha''$. How can one control β? By changing liner thickness at the curvature discontinuity. As a first approximation, the changes in the thicknesses do not

change the forces applied to the liner. However, they do significantly affect the relative velocity of the two liner parts, which produces the plastic flow in this region. Thus, by changing the relative thicknesses of the two parts, one can control the orientation of the necking plane β.

What part should be thicker? In order to increase the hollow penetrator robustness the tendency should be to increase the thickness of the peripheral part. In addition, increases in thickness proportionally decrease penetrator velocity, which is also an important factor for the hole cleaner application. Thus, the liner's peripheral part was designed to be thicker than the central part.

The employment of this technique alone can break the liner, but it does not assure that the peripheral part would produce a robust penetrator. The following considerations were employed in the design of the robust penetrator shown in figure 4b. Near the explosive charge boundary, the detonation products are free to escape into free air, which causes the detonation pressure to be relieved very quickly. When this occurs, the amount of momentum transferred to the liner is degraded, primarily, at the liner's periphery. This has an adverse effect on the formation of the peripheral penetrator resulting in excessive stretching that leads to the formation of the peripheral penetrator resulting in excessive stretching that leads to the formation of a conoidal debris cloud instead of the desired robust penetrator (fig. 4a). The amount of momentum transferred to the liner periphery can be increased with a steel confinement ring. The confinement ring prevents the rapid escape of the detonation products, which enhances the momentum transfer to the liner's periphery and contributes to formation of a robust penetrator. Weickert and Gallagher (ref. 11) investigated a number of confinement ring parameters including length, thickness, and position; our choice of these parameters was very similar to their findings. When a confinement ring was added to a previous design and a proper choice of the liner angles α' and α'' was made, numerical simulations indicated formation of the robust penetrator shown in figure 4b.

Hole Cleaner and Idealized Two-Mass System

The hole cleaner is formed from liner peripheral portion (fig. 4b) via complex plastic deformation, which is simultaneous with translation along the axis of symmetry. In this process, the liner response is rather complex: liner, which is initially a shallow elliptical shell, is subjected to more then 90-deg inversion into a conoidal shell that undergoes gradual changes in shape. To idealize this complex motion, we represented the liner as a two-mass system shown in figure 5. In this two-mass system, masses m_1 and m_2 represent the total liner mass (the peripheral portion) and are placed at liner edges with liner angles α_1 and α_2, respectively. Viscous dampers d_1 and d_2 (fig. 5b) oppose radial motion of masses m_1 and m_2, and model liner resistance to radial collapse. Since during plastic deformation liner can stretch, the masses are thought to be connected through a viscous damper d_3, which permits the distance between the masses to change.

The total momentum transferred from the explosive to liner can be represented with the masses m_1 and m_2 given initial momenta M_1 and M_2, respectively. The ensuing motion of this relatively simple system is governed by a limited number of parameters (initial momenta M_1 and M_2; and damper viscosities); therefore, from the analogy with the motion of this idealized system, one can examine a number of important correlations that can guide liner design. For liner design problems, in which liner design changes are limited only to small changes in liner shape, the primary parameter determining projectile shape is the direction of the impulse delivered from explosive to

liner. Damper viscosities are parameters that model liner strength and relate the deformation resistive forces to displacements produced due to liner plastic flow. Presence of the dampers d_1, d_2, and d_3 in a model is crucial for analysis of a number of the hole cleaner parameters including the radial stability and the length. However, in a liner shape design problem where the concern is with the relationships between liner shape changes and the shape of the resulting penetrator, all the dampers can be omitted and the model can be substantially simplified. This approximation is justified because for small changes in liner shape, the changes in the dissipative forces modeled by dampers d_1, d_2, and d_3 are small and can be neglected. Therefore, for such a model, viscous dampers d_1 and d_2 are omitted and a rigid link is substituted for damper d_3 (fig. 5c). Their shape design problem can then be examined by drawing analogy between changes in liner geometry and variations in momenta M_1 and M_2 of an equivalent two mass system.

Effect of Small Liner Shape Changes

Consider an axisymmetric liner surface in contact with the explosive, which is given by a parametric curve

$$R(\xi) = \varphi_1(\xi)R_1 + \varphi_2(\xi)R_2 + \psi_1(\xi)\dot{R}_1 + \psi_2(\xi)\dot{R}_2$$

where $0 \le \xi \le 1$ is a dimensionless coordinate along the curve $R(\xi) = r(\xi)e_r + z(\xi)e_z$, R_1 and R_2 are vectors at the end points (i.e., at the liner edges), $\dot{R}_1$ and $\dot{R}_2$ are the tangents at these points, and $\varphi_1(\xi), \varphi_2(\xi), \psi_1(\xi)$, and $\psi_2(\xi)$ are arbitrary blending functions such as

$$\begin{aligned}
&\varphi_1(0) - 1, \varphi_1(1) = 0 \\
&\varphi_2(0) = 0, \varphi_2(1) = 1 \\
&\dot{\varphi}_1(0) = \dot{\varphi}_1(1) = \dot{\varphi}_2(0) = \dot{\varphi}_2(1) = 0 \\
&\dot{\psi}_1(0) = 1, \dot{\psi}_1(1) = 0 \\
&\dot{\psi}_2(0) = 0, \dot{\psi}_2(0) = 0 \\
&\psi_1(0) = \psi_1(1) = \psi_2(0) = \psi_2(1) = 0
\end{aligned}$$

Now consider a liner design problem, in which liner shape is changed in small increments. Consider that these small changes in liner profile are carried out through small changes in edge axial positions z_1 and z_2 (fig. 6a) and/or liner angles $\tan\alpha_1 = \dot{r}_1 / \dot{z}_1$ (fig. 6b) and $\tan\alpha_2 = \dot{r}_2 / \dot{z}_2$, while the radial positions r_1 and r_2 of the edges are fixed. Further, suppose that blending functions are such that the resulting liner profile is a smooth, small curvature function. Clearly, when z_1, z_2, and/or α_1 or α_2 are changed, both $R(\xi)$ and $\tan\alpha(\xi) = \dot{r}(\xi)/(\dot{z}(\xi))^{-1}$ change. Since projectile formation is extremely sensitive to liner profile changes, the extent of variation δR arising from small variations $\delta z_1, \delta z_2, \delta\alpha_1$, and $\delta\alpha_2$ must be discussed thoroughly.

First, consider the magnitude of the total momentum transferred to the liner, which can be expressed as

$$M_0 = 2\pi \int_0^1 \int_0^\tau p(\xi, t) r(\xi) d\xi dt$$

where t is the time, $p(\xi,t), t<\tau; p=0, t>\tau$ is the pressure exerted on the liner by the explosive. Since the momentum is directly proportional to the radial component $r(\xi)$ of liner profile, the primary effects of liner shape changes are the variations δr.

Consider first that the effect on changes δz_1 and δz_2 in the axial positions of the liner edges (fig. 6a). Since

$$r(\xi)=\varphi_1(\xi)r_1+\varphi_2(\xi)r_2+\psi_1(\xi)\dot{r}_1+\psi_2(\xi)\dot{r}_2$$

clearly, $\delta r(\xi,\delta z_1,\delta z_2)=0$. Now consider a situation where liner profile is adjusted by changing the liner angle α_1 (fig. 6b). Since a small change $\delta\alpha_1$ changes only the direction of the tangent vector $\dot{R}_1=\|\dot{R}_1\|e_{t1}$, the resulting variation in position of point ξ due to a change $\delta\alpha_1$ is

$$\delta R(\xi,\delta\alpha_1)=\psi_1(\xi)\|\dot{R}_1\|\,\delta(e_{t1})$$

Noting that the rotational change of the unit vector e_{t1} is given by

$$\delta(e_{t1})=\delta\alpha_1 e_q\times e_{t1}$$

the variation in liner profile is then

$$\delta R(\xi,\delta\alpha_1)=\psi_1(\xi)\|\dot{R}_1\|\,\delta\alpha_1 e_q\times e_{t1}$$

Figure 6c illustrates typical shapes of the blending function $\psi_1(\xi)$. For smooth, small curvature profiles $\psi_1(\xi)\langle\langle 1$. From figure 6d, it can be shown that

$$\delta r(\xi,\delta\alpha_1)\approx\upsilon_1(\xi)\|\dot{R}_1\|\,\delta\alpha_1\cos\alpha_0$$

where angle α_0 is defined in figure 6d and $\arctan((r_2-r_1)/(z_2-z_1))<\alpha_0<\alpha_1$. For typical shallow liner profiles, $\cos\alpha_0$ is small. Thus, for $\psi_1(\xi)\langle\langle 1$ and small $\delta\alpha_1$, $\delta r(\xi,\delta\alpha_1)$ is negligible. Similarly, it can be shown that $\delta r(\xi,\delta\alpha_2)$ is also small, and we conclude that any small liner shape adjustments δz_1, δz_2, $\delta\alpha_1$, and $\delta\alpha_2$ do not affect $r(\xi)$.

Now consider the changes in pressure profile $p(\xi,t)$ due to small liner shape changes. Since the radial variations δr are negligible, a change in pressure at the interface between the explosive and the liner can be only due to the axial variations δz. A typical pressure history at a point at the interface between the explosive and the liner can be generically represented by a curve rapidly decreasing off a Chapman-Jouguet state. The profile of this curve reflects the pattern of interaction of rarefaction waves originated along the entire charge boundary, including the liner free surface. With a change in the geometry of a boundary, the distances traveled by the rarefaction waves change; therefore, any liner profile modifications are expected to affect the profile of the pressure history.

When the charge diameter is fixed, the most significant change in the boundary is in the axial position of the liner free surface. Undoubtedly, this changes the time of arrival of the detonation wave at the explosive liner interface. For example, for a plane detonation wave propagating with a velocity D_0, a change in the detonation wave time of arrival is given by

$$\delta T = \frac{\delta z}{D_0}$$

For small δz and a shallow liner profile, relative changes in distances between pairs of arbitrary points at the interface between the explosive and the liner are negligible. Therefore, it is reasonable to assume that the pressure history profile is not significantly affected by a small change in the liner free surface. Hence, the pressure for a modified liner can be expressed as

$$p(\xi, t+\delta T) \approx p(\xi, t)$$

Similar assumptions can be applied to the relaxation time τ, which is also expected not to vary significantly with slight changes in the liner geometry. Thus, the value of the integral

$$\int_0^{\tau} p(\xi, t)\, dt$$

will be unchanged. Since $r(\xi)$ is not affected by small changes in liner geometry, we can conclude that the magnitude of the total momentum M_0 transferred to the liner is invariant to slight liner modifications.

The radial and the axial components of the total momentum are given as

$$M_{0r} = 2\pi \int_0^1 \int_0^{\tau} p \cos\alpha(\xi)\, r(\xi)\, d\xi\, dt$$

$$M_{0z} = 2\pi \int_0^1 \int_0^{\tau} p \sin\alpha(\xi)\, r(\xi)\, d\xi\, dt$$

With adjustments in liner shape, the liner angle $\alpha(\xi)$ can change substantially, which effects the ratio between the axial and the radial components of the momentum transferred to the liner. Thus, the primary effect of small liner shape adjustments is to change the direction of the total momentum, while its magnitude remains the same. Similarly, we suggest that liner shape adjustment carried out by changing liner angles α_1 and α_2 is analogous to changing the "ratio" between the momenta M_1 and M_2 of the two-mass system, while their total magnitude is fixed. Results of numerical simulations shown in figure 7 and discussed next confirm the validity of this analogy.

Numerical Simulations of Effects of Small Liner Shape Changes on Hole Cleaner

Refer to figure 7a through e, which shows the effects of small liner geometry variations on hole cleaner design, all calculated at 130 μs. All liner shape adjustments presented here were achieved by changing peripheral liner thickness and liner angles α_1 and α_2, while the radial positions of the outer edge and the central portion (that produces the hole driller) were fixed. It is interesting to note that all calculations give essentially identical hole driller shapes. This illustrates the usefulness of the employed charge design rationale that is based on a concept of mutual independence of the formation processes of the hole driller and the hole cleaner.

Figure 7a presents calculations wherein liner angle α_2 was changed by 5 deg, which produced approximately 16% relative radial "translation" of the hole cleaner. This liner profile was designed using a small axial shift of the liners outer edge, while α_1 and liner thickness were fixed. This type of liner shape adjustment can be expressed as $\alpha(\xi)\pm\gamma$, where depending on the shift direction, the liner angle is either increased or decreased by an angle γ. For typical liner profiles with $60° < \alpha(\xi) < 90°$ and small γ

$$\sin(\alpha \pm \gamma) \approx \sin(\alpha)$$
$$\cos(\alpha \pm \gamma) \approx \cos(\alpha) \mp \gamma, \quad 60° < \alpha(\xi) < 90°, \text{ small } \gamma$$

with a maximum of 12% error bound. The magnitudes M_{0r} and M_{0z} are directly proportional to the values of $\sin(\alpha \pm \gamma)$ and $\cos(\alpha \pm \gamma)$, respectively, therefore, we can draw a conclusion that such adjustments can only change the radial component of the momentum, while the axial component remains approximately the same. Thus, the radial translation effect observed in figure 7a is due to changes in the radial component of the momentum, which caused significant change in the hole cleaner diameter. In terms of the idealized two-mass system, such liner shape adjustment is equivalent simply to a proportional change of both M_{1r} and M_{2r} while $\|M_1\| + \|M_2\|$ is fixed.

From penetrator design considerations, it can be desirable to decrease the hole cleaner velocity without affecting its shape. From an analogy with the idealized two-mass system, a simple solution is to proportionally change both masses m_1 and m_2; in a liner design this can be readily implemented by changing liner thickness. Figure 7b compares two designs with identical liner profiles and different thicknesses. Results in figure 7b show a distinct difference in the axial position of the two hole cleaners produced from these designs, while their shape is essentially the same.

Consider another hole cleaner design problem in which the desired shaped is a hollow cylinder. Using the two-mass system analogy, a poor penetrator shape can be explained from the motion of the idealized masses m_1 and m_2. Motion of these masses can be viewed as a "clockwise" rotation about their center of mass combined with the center of mass translation. As seen in figure 7, at 130 μs the penetrator had formed in a way that its wall is at some angle with the z axis. In order to increase this angle to the desired 180 deg, the liner wall rotation rate should be changed.

Let us now consider the factors affecting the liner wall rotation rate. First, consider the idealized two-mass system. Conservation of angular momentum requires that

$$g = \frac{dH}{dt}$$

The torque G that is initially imparted to the masses can be expressed as

$$G_0 = le_1 \times (\xi_{cm} F_1 - (1 - \xi_{cm}) F_2)$$

where $F_1 = \partial M_1 / \partial t, F_2 = \partial M_2 / \partial t, \xi_{cm}$ is the position of the center mass of the system of masses m_1 and m_2, and l is the distance between the masses, whose relative orientation is given by a unit vector e_1. After the initial angular impulse is delivered to the system, and in the absence of dissipative forces, $G = 0$. Hence, integrating the angular momentum balance equation yields the rotational rate

$$I\dot{\omega} = H(0)$$

where I is rotational inertia of the system. The angular momentum $H(0)$ at $t = 0$ can be expressed as

$$H(0) = le_1 \times \left(\xi_{cm} \int_0^\tau F_1 dt - (1 - \xi_{cm}) \int_0^\tau F_2 dt \right)$$

or simply

$$H(0) = le_1 \times (\xi_{cm} M_1 - (1 - \xi_{cm}) M_2)$$

Thus, for a given system with fixed ξ_{cm}, the magnitude of the angular momentum depends on the vector difference between the momenta M_1 and M_2. Therefore, the system rotation rate can be varied by changing relative directions of momenta M_1 and M_2. Angular momentum transferred to a liner is

$$H = 2\pi \int_0^1 \int_0^\tau pr(\xi)(R(\xi) - R_{cm}) \times n(\xi) d\xi dt$$

where $n(\xi)$ is a unit normal of liner surface, R_{cm} is the position of the liner center of mass, and $R(\xi) = r(\xi)e_r + z(\xi)e_z$. Let us assume that for these liner design problems, small changes in liner shape $R(\xi)$ produce negligible changes in angular inertia. Thus, similarly to the two-mass system, where a change in rotation rate is achieved by changing the momenta directions, the rate of the liner wall rotation can be influenced primarily by changing the liner surface orientation $n(\xi)$.

In design E shown in figure 7c, the shape of the original liner C was changed using an approximately 5-deg increment (α_1) and decrement (α_2) of the liner edge angles, while the positions of both edges were fixed. Note, that since the "average" liner angle $\frac{1}{2}(\alpha_1 + \alpha_2)$ remained the same, the total momentum (linear momentum) transferred to the liner was unchanged. However, due to the higher liner curvature of design E, the total angular momentum transferred to the liner was increased. Calculated penetrator shapes produced from the designs E and D are compared in figure 7c. In agreement with the previous discussion, an increase of the angular momentum increased the liner wall rotation, and figure 7c shows that the wall of design E "straightened up." In this particular design, liner D is lighter than E, therefore, the position of liner D is slightly shifted to the right. Figure 7d compares the design E with design F, which has the same thickness, but substantially different curvatures (due to an approximately 11 deg difference between the corresponding liner edge angles). In this case, the difference between liner curvatures is much higher, and the effect of rotation rates is even more pronounced.

In the preceding discussion, we omitted all viscous dampers from the two-mass system. Let us first consider the effect of the viscous damper d_3, which models liner stretching and permits the distance between the masses to change. If in the idealized two-mass system the rigid link between masses is released (i.e., replaced with a damper with zero viscosity), the stretching rate can be expressed as

$$\dot{\varepsilon} = \frac{M_1 \cdot e_1}{m_1} - \frac{M_2 \cdot e_1}{m_2}$$

Since the rate of stretching is proportional to the relative difference between the velocities of the masses, changing the mass ratio effects stretching. In the designs E and D, we changed liner thickness uniformly by 5%, which resulted only in slight changes of the center of mass velocity (fig. 7b). Now, consider design G whose liner angle profile is identical to E, but the thicknesses are different: at edge 1 by 57% and at edge 2 by the same 5% (as in designs E and D). Calculations of hole cleaner shapes produced from these designs are compared in figure 7e. Calculations show not only increases in the center of mass velocity, but in addition, a significant increase in length. Since, in general, penetrator effectiveness is enhanced with increased in length, this might be a useful factor to consider in designing hole cleaners.

A requirement that is important for the effectiveness of a hole cleaner is its radial stability; i.e., after the desired hollow cylinder with equal front and rear diameters D_1 and D_2, respectively, if formed, radial deformations should cease. As discussed, formation of the hole cleaner is accomplished through rotation of the liner wall, and liner rotation with continue until the angular momentum initially imparted to the liner is dissipated in plastic flow. Several suggestions to obtain a radially stable design can be offered. Consider that the design objective has produced a hole cleaner with given diameter D at a given standoff (or formation time). The first step will be to design a liner that produces a penetrator with front diameter $D_1 \approx D$ at which time the liner rotation has ceased. In terms of the two-mass system, such a design can be obtained by proper balance between the damper viscosities d_1 and d_2, and the initial amount of the angular impulse delivered to the system. Since the damper viscosities represent the forces resisting plastic deformation, the corresponding liner parameters are the liner material strength and thickness. Suppose that such a design is achieved, but $D_2 > D_1 \approx D$. Once such a design id established, the second step is to try increasing

the hole cleaner wall rotation by changing liner curvature. This is quite feasible, since in the result shown in figure 7d more than a 45-deg rotation change (with the rotation still continuing) was achieved by an 11-deg change in the liner edge angles. Changing liner curvature might also disturb the achieved balance between angular impulse and dissipation, which might result in $D_1 > D$. When $D_1 > D$ occurs, we continue iteration from the first design step and try to decrease D_1 by increasing liner thickness. To achieve a suitable design will definitely require more than one design iteration and the performance of each iteration should be verified experimentally.

EXPERIMENTS

The explosive charge was cast from molten Octol 70/30 explosive using a sedimentation technique. This technique allows the gravity settling of heavier HMX particles in the melted explosive, which permits a higher concentration of more energetic HMX particles in the main portion of the charge (close to the liner), while the less energetic TNT flows upward toward the riser.

The charge casting procedure was as follows:

The device was assembled from the aluminum casing, the liner, and the steel confinement ring, which were bonded together using an adhesive. The Octol 70/30 explosive was melted and heated to approximately 96° to 104°C. A vacuum about 686 mm of Mercury was applied to the melt kettle for 15 min. The explosive was poured into the preheated charge assembly and vibrated for 10 min. The assembly was maintained at a minimum temperature of 96°C for at least 1.5 hrs. Compressed air at ambient temperature was then applied to the liner surface while the riser was maintained above 93°C. This allowed the explosive to solidify from the liner upward toward the riser. The heat source to the riser was later removed, and the charge was allowed to cool slowly to ambient temperature. The loading funnel and the riser were then removed and the surface of the explosive was hand smoothed to final design dimensions. The 1.9-cm long and 2.54-cm diameter CH-6 booster pellet was placed into a cylindrical cavity (0.3-cm deep) machined in the cast explosive. A Reynolds RP-2 detonator was centered on the booster with a machined detonator holder.

The objective of this experiment was to prove the feasibility of producing two robust penetrators from a single charge. Therefore, clear images of the penetrator's shape during projectile formation (starting from a relatively early time) were crucial to the success of the experiment. The following considerations motivated the usage of flash (i.e., short exposure) radiography. The explosion generates an opaque cloud of detonation products and miscellaneous debris, which blocks the projectile's view at early projectile formation times. This phenomenon limits the utility of optical photography. The density of the debris cloud is low, so that the cloud is transparent even to low intensity x-ray radiation. This makes flash radiography ideally suited for this experiment. As the penetrator formed, three x-ray tubes exposed x-ray film, which recorded the projectile images.

A schematic of the experimental setup is shown in figure 8. The equipment was conducted inside an explosion proof chamber. The three x-ray tubes were installed in special ports in the wall and in the ceiling of the chamber. X-ray tube A (fig. 8) was installed in the ceiling, directed to the x-ray film cassette A, and provided the top view of the penetrator. The x-ray tubes B and C were installed in the same wall port and provided two side views of the penetrator. Tubes B and C were positioned in a plane orthogonal to the projectile path and at an angle to each other (tube C was in a horizontal plane). Tubes B and C were pointed to the same cassette B; the lower portion of the cassette recorded the image from tube B; while the upper portion – from tube C.

The x-ray port positions are fixed in the explosion chamber, and they had to be used in a way that provided the fullest views for certain x-ray exposure times. On the other hand, the desired exposure times have to represent characteristic stages of projectile formation. Thus, x-ray exposure times of 105 μs and 200 μs were selected as a compromise between the fixed x-ray port positions and the desired times based on the numerical simulations. These times were used to trigger x-ray tubes A and B, respectively. The third x-ray exposure at 220 μs (for tube C) was set a short time after the second exposure, which was necessary for the reliable measurement of projectile velocities.

The longitudinal position of the charge in the chamber was selected in reference to the first x-ray port position (tube A) and was based on the projectile velocities calculated in the numerical simulations. The charge was positioned in a light Styrofoam stand. A stack of fifteen 25.4 x 25.4-cm square 5-cm thick steel witness plates was positioned 109 cm from the edge of the charge on an auxiliary wood frame, which also supported the charge stand. A 7.5-cm diameter steel calibrating rod, with fiducial marks 5 cm apart, was positioned along the expected projectile's path. The film was then irradiated with a small doze, which reproduced the pattern of fiducial marks on the film. This produced a convenient spatial reference frame, which simplified data reduction procedures such as the reference of the image positions, the x-ray magnification factors, etc. After the exposure, the calibrating rod was removed. During the experiment, the films were exposed again and the projectile's images were superimposed with the images of the fiducial marks.

The radiographic images of the penetrator exposed at 105 μs, 200 μs, and 220 μs are shown in figure 9. All radiographs show that the liner separated into two robust parts. At 105 μs, the site of separation is still well preserved on the central portion of the projectile. The characteristic shape of this site resulted from intensive plastic flow (i.e., necking) in the vicinity of the liner curvature discontinuity, and it agrees very well with the numerical simulations (figs. 4 and 7). The later radiographs of 200 μs and 220 μs indicate formation of a ring of debris at the site; i.e., the material which formed that neck had fractured.

In order to trace the evolution of the projectile shape with time, four characteristic points were identified (fig. 9): points 1 and 2 represent an idealized shape of the home cleaner; points 3 and 4 are the respective positions of the tail and the tip of the hole driller. Tabulated $r - z^*$ coordinates of these points are given in figure 9. The evolution of penetrator shape agrees very well with the results predicted from the numerical simulations. Based on radiographs at 200 μs and 220 μs, the tip and the tail of hole driller mover with velocities 4.3 km/s and 0.9 km/s, respectively. These velocities agree very well with the numerical simulations.

Based on the data in figure 9, the average axial velocity of point 1 (the front) of the hole cleaner between 105 μs and 200 μs was 2.93 km/s, while between 200 μs and 220 μs it was 2.90 km/s. In the same time, the axial velocity of point 2 (the rear of the hole cleaner) increased from 2.55 km/s to 2.70 km/s. These data agree very well with the tendencies observed in the numerical simulations: formation of the hole cleaner is accomplished through a deceleration of the front and acceleration of the rear. As the hole cleaner continues to form, the radial velocities of its rear and front change from –0.18 km/s to –0.10 km/s and from –0.24 km/s to +0.05 km/s, respectively. The data indicate significant rotation of the hole cleaner, which confirms the formation mechanism observed in numerical simulations. When the rotation reaches a pint when the diameter of the penetrator front starts to increase (i.e., the front starts to stretch circumferentially), it adversely affects the robustness of the hole cleaner. Ultimately, this rotation will lead to the fracture of the hole cleaner.

A photograph of the first four witness plates and a schematic of the hole profile are given in figure 10, which shows two distinct hole portions produced by the hole driller and by the hole cleaner. Since the hole produced by the cleaner is well rounded and symmetrical, it is assumed that the penetrator did not fracture. On the other hand, because of the continuing rotation, the performance of the hole cleaner was degraded. The supporting considerations are as follows: The target was located approximately 40 cm from the position of the last radiographic image (220 μs) of the hole cleaner and at this time its length was 6.7 cm. Based on ideal hydrodynamic theory of penetration (ref. 1), the penetration depth can be approximately estimated as $P = L\sqrt{\rho_p / \rho_t}$, where L is the length of the penetrator and ρ_p and ρ_t are the densities of the penetrator and the target. If the hole cleaner was stable, simple calculations give an estimate for penetration to be at least 7.2 cm, which is approximately 40% deeper than the depth witnessed in the experiment. Thus, we conclude, that at the time of the encounter with the target (≈360 μs) the hole cleaner length was degraded to approximately 4.7 cm. The reason for this decrease in length was continuing rotation of the hole cleaner.

CONCLUSIONS

Rapid hole boring for demolition operations requires a complex penetrator consisting of two separate parts: a hole driller and hole cleaner. To produce this complex penetrator from a single charge is not a simple task. We provide the validity of a liner design rationale wherein formation of the hole driller and hole cleaner are mutually independent, and their shape can be adjusted using incremental changes in liner profile. We identified a number of parameters tat are crucial for preventing liner fracturing during separation into two parts and ensuring the robustness of the resulting penetrator. The experiments proved the validity of the approach and indicated the feasibility of producing a robust penetrator of this complex shape. The hole driller produced in the experiments is quite satisfactory for the hole boring, while the hole cleaner requires additional adjustment. The deficiencies of the achieved hole cleaner design (such as poor shape and radial instability) are typical for many interim hole cleaner design that were observed in numerical simulations and discussed in this work. Formation of the hole cleaner is accomplished through rotation of the liner wall, and this rotation continues until the angular momentum initially imparted to liner is dissipated in plastic flow. Since the initial liner angular impulse and its dissipation can be controlled by adjustments in liner profile and thickness, a suitable design may be achieved via proper incremental liner shape changes. This may be accomplished using a number of techniques developed in this work and would require a few analytical and experimental design iterations.

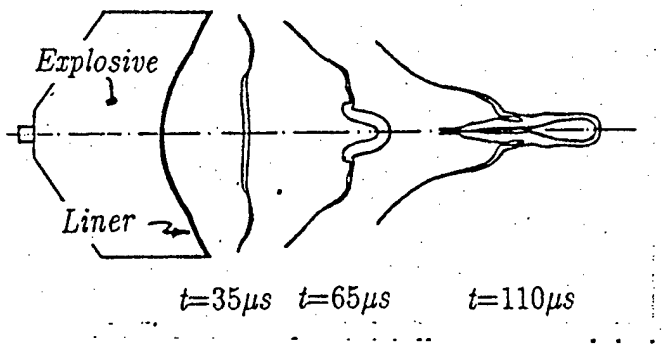

Figure 1
Numerical simulations of an initially attempted design
Both the central and the peripheral parts of the penetrator are unsatisfactory.

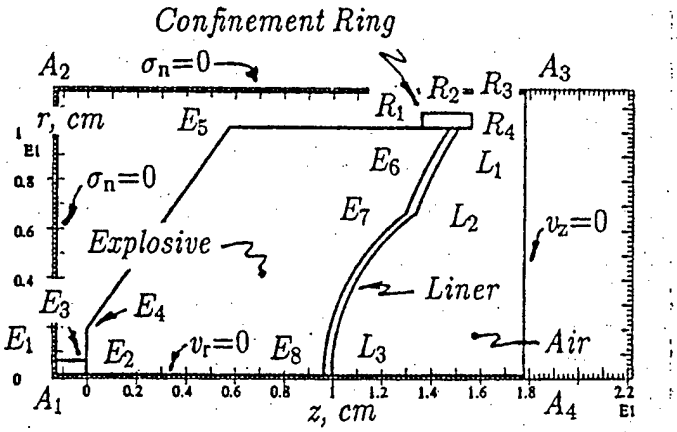

Figure 2
Initial configuration of explosive charge and liner

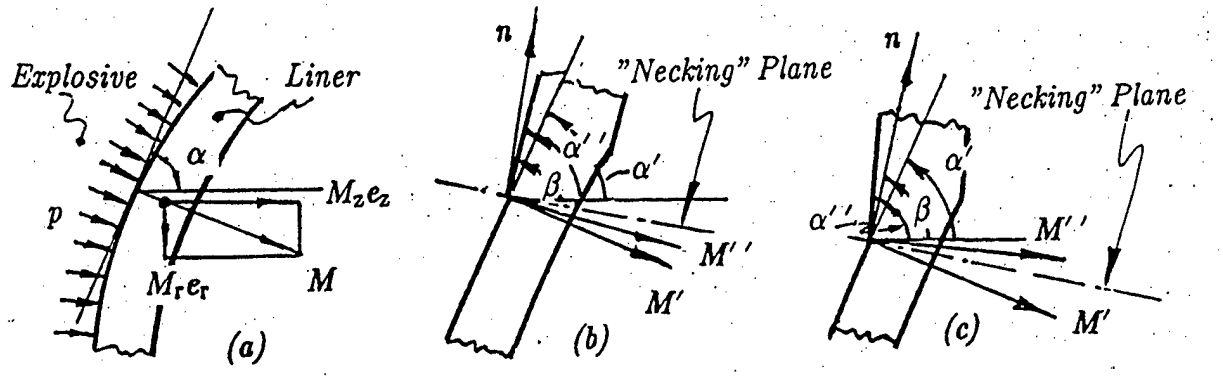

Figure 3

The adjustment of the liner angle α is a common technique for control of liner collapse and projectile formation

Changing liner angles α' and α'' and the orientation of the necking plane β, one can control liner separation into two pats. The liner in (b) does not satisfy the condition for liner separation ($\alpha' < \beta < \alpha''$), while the liner in (c) does.

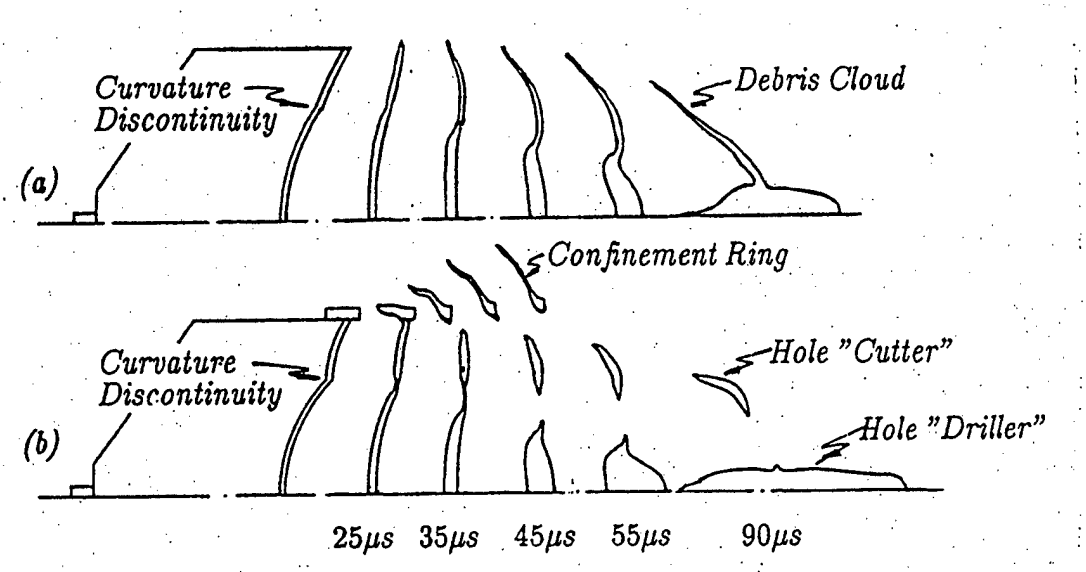

Figure 4

Numerical simulations of liner collapse and projectile formation

Design (a) resulted in excessive stretching of the peripheral penetrator, which led to formation of a conoidal debris cloud instead of the desired robust penetrator. Design (b), which produced a robust hole cleaner and stretching hole driller, is quite satisfactory

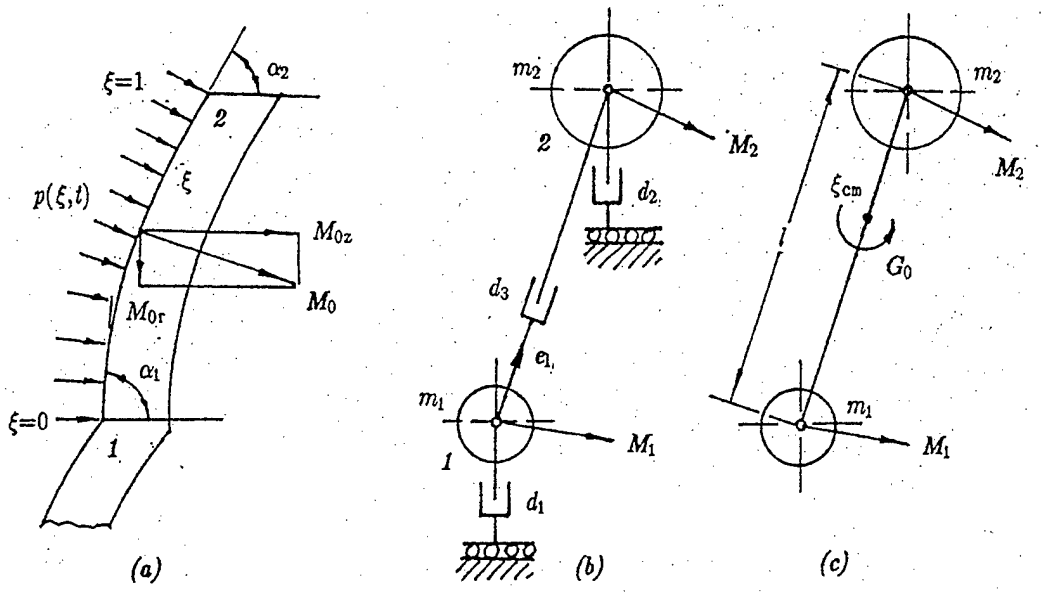

Figure 5

Liner peripheral portion can be represented as an idealized two-mass system with masses m_1 and m_2 placed at the edges 1 and 2

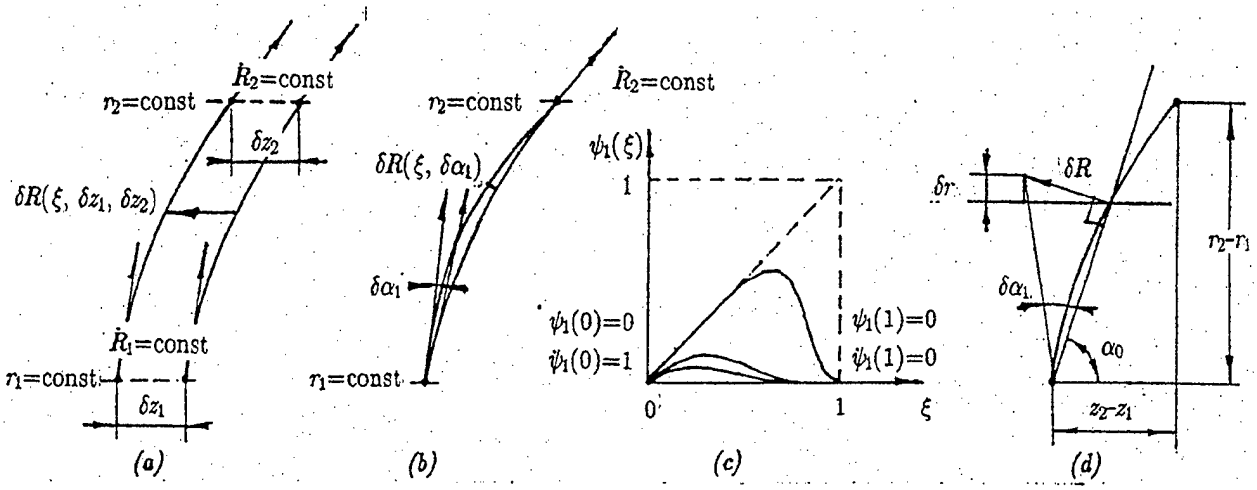

Figure 6

Liner profile can be changed by small changes in edge axial position δz_1 and δz_2 (a) and in a liner edge angle α_1 (b), while the radial positions r_1 and r_2 of the edges are fixed

Small adjustments $\delta\alpha_1$ in liner edge angle α_1 result in negligible radial changes δr of the liner profile.

Design	α_1	α_2	t_1	t_2
	degrees		cm	
A	80	74	0.388	0.388
B	80	69	0.388	0.388
C	81	63	0.388	0.349
D	81	63	0.370	0.330
E	87	58	0.388	0.349
F	81	63	0.370	0.330
G	87	58	0.218	0.333

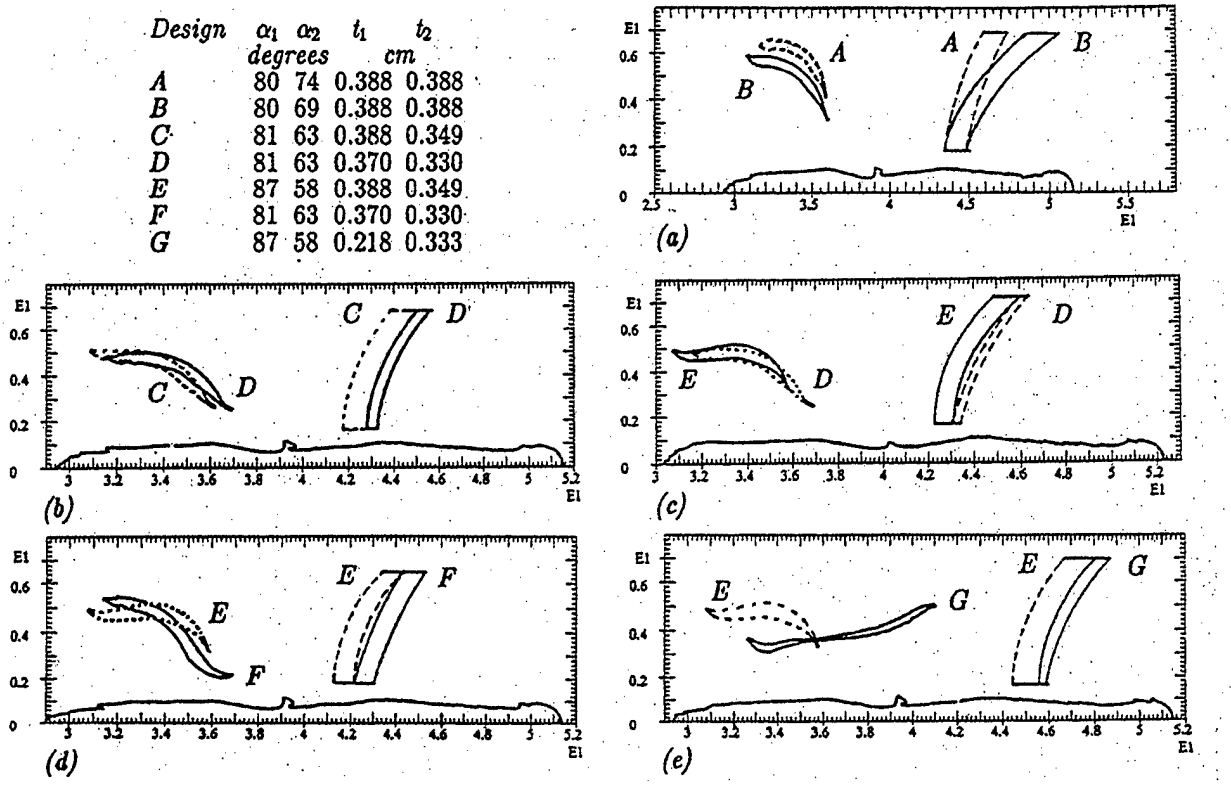

Figure 7
Calculated hole cleaner shape changes due to changes in liner (peripheral portion) profile

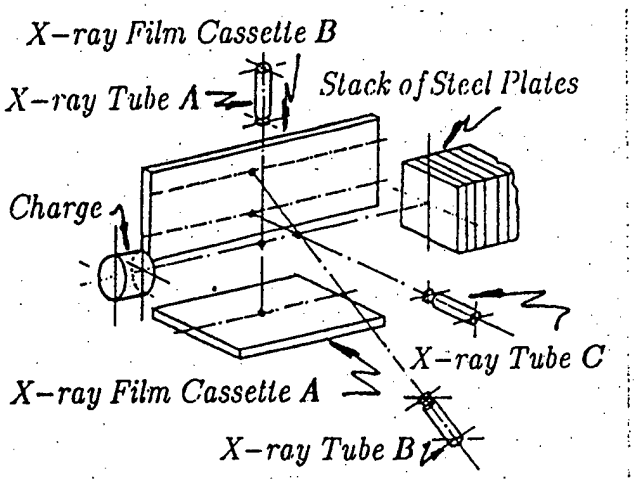

Figure 8
Schematic of the experimental setup

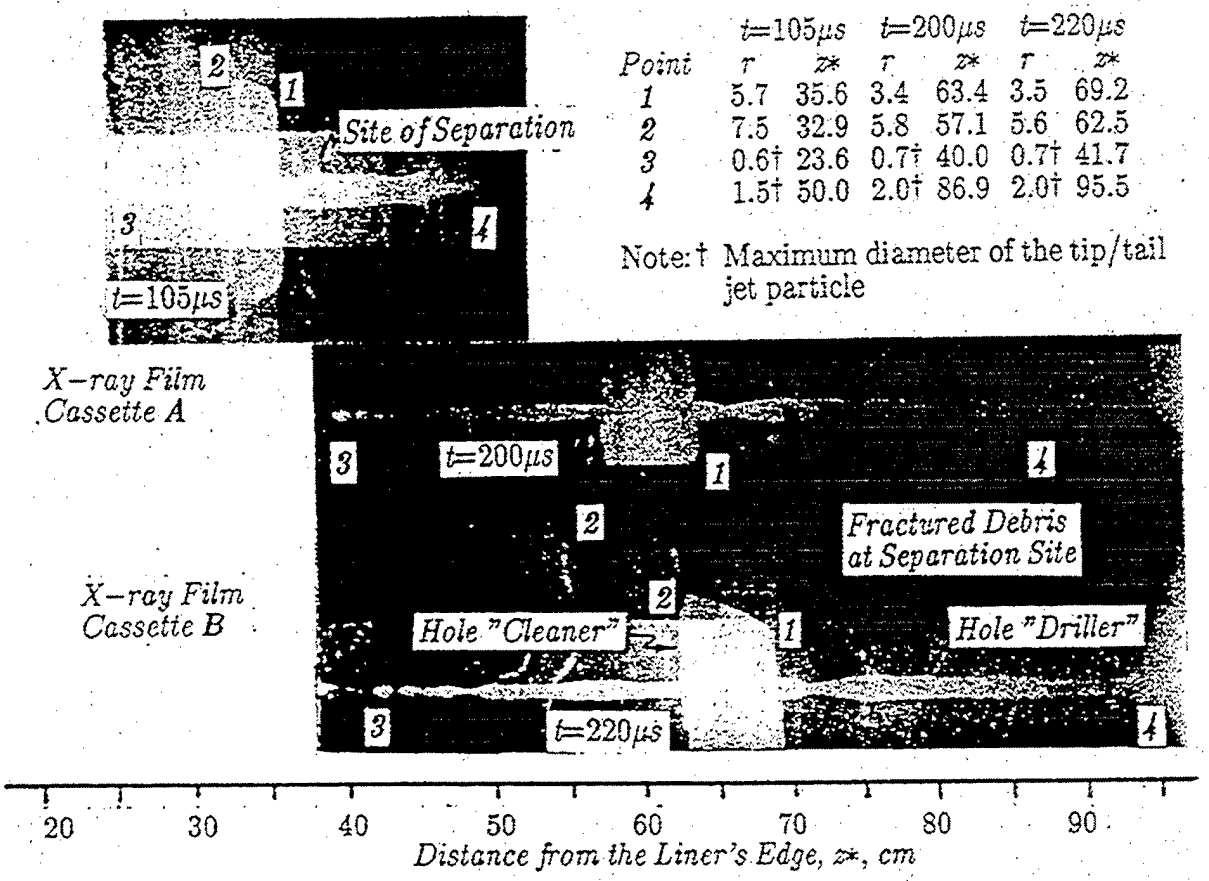

Point	t=105μs r	t=105μs z*	t=200μs r	t=200μs z*	t=220μs r	t=220μs z*
1	5.7	35.6	3.4	63.4	3.5	69.2
2	7.5	32.9	5.8	57.1	5.6	62.5
3	0.6†	23.6	0.7†	40.0	0.7†	41.7
4	1.5†	50.0	2.0†	86.9	2.0†	95.5

Note: † Maximum diameter of the tip/tail jet particle

Figure 9
Radiographic images of the projectile show that the liner formed a robust hole cleaner and a stretching hole driller

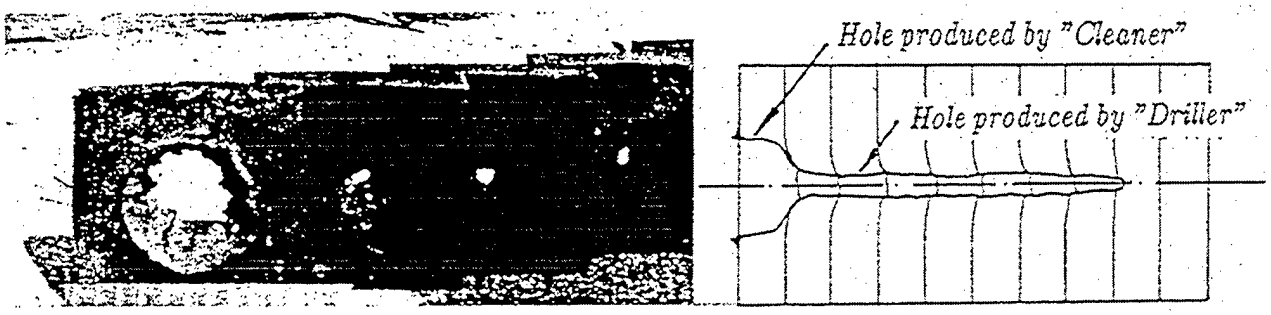

Figure 10
Photograph of a schematic of the hole produced in a stack of steel witness plates

REFERENCES

1. Birkhoff, G.; MacDougall, D. P.; Pugh, E. M.; and Sir Taylor, G., "Explosive with Lined Cavities," J. Appl. Phys., Vol. 19, No. 6, pp. 563-582, 1948.

2. Kennedy, D. R., "History of the Shaped Charge Effect," D. R. Kennedy & Associates, Mountain View California, 1983.

3. Hornemann, U.; Schroder, G.-A; and Weimann, K., "Explosively-Formed Projectile Warheads," Military Technology, No. 4/87, pp. 36-50, 1987.

4. Weinmann, K., "Flight Stability of EFP with Star Shaped Tail," Proc. of the 14th International Symposium on Ballistics, Quebec, Canada, pp. 755-763, 1993.

5. Rosner, H., "Optimization of Shaped Charges Against Concrete Targets," Proceedings of the Sixth International Symposium on Interaction of Nonnuclear Munitions with Structures, Panama City Beach, Florida, pp. 273-276, 1993.

6. Gold, V. M.; Pearson, J. C.; and Turci, J. P., "A Study of Impact Response of Concrete and Reinforced Concrete Targets for the Velocities Circa 0.2 cm/μs," Proceedings of the International Symposium on Impact Engineering, Vol. 1, Sendai, Japan, pp. 217-222, 1992.

7. Tipton, R. E., "CALE Users Manual," Version 910201, Lawrence Livermore National Laboratory, 1991.

8. Wilkins, M. L., "Calculations of Elastic-plastic Flow," In: B. Adler, S. Fernbach, and M. Rotenbert (eds), Methods of Computational Physics, Vol. 3, Academic Press, New York, pp. 211-263, 1964.

9. Wilkins, M. L., "Calculations of Elastic-plastic Flow," UCRL-7322, Rev. 1, Lawrence Livermore National Laboratory, 1969.

10. Steinberg, D. J.; Cochran, S. G.; and Guinan, M. W., "A Constitutive Model for Metals Applicable at High-strain Rate," J. Appl. Phys., Vol. 51, No. 3, pp. 1498-1504, 1980.

11. Tipton, R. E., "EOS Coefficients for the CALE Code for Some Materials," Lawrence Livermore National Laboratory, 1991.

12. Weickert, C. A. and Gallagher, P. J., "Parametric Study of the Effect of a Confinement Ring on the Shape of an Explosively Formed Projectile," Proc. of the 13th International Symposium on Ballistics, Stockholm, Sweden, pp. 228-237, 1992.

BIBLIOGRAPHY

1. Weimann, K., "Modelling, Testing, and Analysis of EFP Performance as a Function of Confinement," Proc. of the 12th International Symposium on Ballistics, San Antonio, Texas, pp. 228-237, 1990.

2. Weimann, K., "Research and Development in the Area of Explosively Formed Projectiles Charge Technology," Propellants, Explosives, Pyrotechnics, Vol. 18, pp. 294-298, 1993.

DISTRIBUTION LIST

Commander
Armament Research, Development and Engineering Center
U.S. Army Tank-automotive and Armaments Command
ATTN: AMSTA-AR-WEL-T (2)
AMSTA-AR-GCL
AMSTA-AR-WEE-C (5)
Picatinny Arsenal, NJ 07806-5000

Defense Technical Information Center (DTIC)
ATTN: Accessions Division (12)
8725 John J. Kingman Road, Ste 0944
Fort Belvoir, VA 22060-6218

Director
U.S. Army Materiel Systems Analysis Activity
ATTN: AMXSY-EI
392 Hopkins Road
Aberdeen Proving Ground, MD 21005-5071

Commander
Chemical/Biological Defense Agency
U.S. Army Armament, Munitions and Chemical Command
ATTN: AMSCB-CII, Library
Aberdeen Proving Ground, MD 21010-5423

Director
U.S. Army Edgewood Research, Development and Engineering Center
ATTN: SCBRD-RTB (Aerodynamics Technology Team)
Aberdeen Proving Ground, MD 21010-5423

Director
U.S. Army Research Laboratory
ATTN: AMSRL-OP-CI-B, Technical Library
Aberdeen Proving Ground, MD 21005-5066

Chief
Benet Weapons Laboratory, CCAC
Armament Research, Development and Engineering Center
U.S. Army Tank-automotive and Armaments Command
ATTN: AMSTA-AR-CCB-TL
Watervliet, NY 12189-5000

Director
U.S. Army TRADOC Analysis Command-WSMR
ATTN: ATRC-WSS-R
White Sands Missile Range, NM 88002

Commander
Naval Air Warfare Center Weapons Division
1 Administration Circle
ATTN: Code 473C1D, Carolyn Dettling (2)
China Lake, CA 93555-6001

GIDEP Operations Center
P.O. Box 8000
Corona, CA 91718-8000